PHYSICAL REVIEW B VOLUME 60, NUMBER 6 1 AUGUST 1999-II

Physical analysis of the state- and rate-dependent friction law. II. Dynamic friction

T. Baumberger* and P. Berthoud[†]
Laboratoire de Physique de la Matière Condensée,[‡] École Normale Supérieure, 24 rue Lhomond, 75231 Paris Cedex 05, France

C. Caroli
Groupe de Physique des Solides,[‡] 2 place Jussieu, 75251 Paris Cedex 05, France

(Received 5 March 1999)

We report an extensive study of dynamic friction at nonlubricated multicontact interfaces between nominally flat bodies, rough on the micrometer scale, made of identical polymer glasses. This work, which complements a previous study of static friction on the same systems, has been performed at temperatures ranging from 20 °C to close below the glass transitions. The data are analyzed within the framework of the Rice-Ruina state- and rate-dependent friction model. We show that this phenomenology is equivalent to a generalized Tabor decomposition of the friction force into the product of an age-dependent load-bearing area and of a velocity-strengthening interfacial shear stress. Quantitative analysis of this latter term leads to associate velocity strengthening with thermal activation of basic dynamical units of nanometer dimensions. We interpret our results with the help of a model due to Persson, in which shear is localized in a nanometer-thick interfacial adhesive layer, pinned elastically at a low shear level. Sliding proceeds via uncorrelated depinning of ‘‘nanoblocks’’ which constitute the layer. It is the competition between the drive-induced loading of these blocks up to their depinning stress and the thermally activated premature depinning events which leads to the velocity-strengthening contribution to the interfacial strength. In our interpretation, friction therefore appears as the localized elastoplastic response of a confined amorphous interfacial layer. [S0163-1829(99)13129-1]

I. INTRODUCTION

The physics of solid friction has benefited from recent progress along two different, though complementary, lines of research.

The first one is concerned with the (quasi)statics and low velocity dynamics of multicontact interfaces (MCI's) between macroscopic solids with rough surfaces. Within this framework, one usually expresses the friction force, following Bowden and Tabor,[1] as

$$F=\sigma_s\Sigma_r\,, \tag{1}$$

where Σ_r is the real area of contact (consisting, for a MCI, of a large number N of microcontacts of average radius $\langle a\rangle$ typically on the order of micrometers), and the stress σ_s defines an interfacial shear strength.

For a MCI, the Amontons-Coulomb proportionality between F and the normal load W then results, as shown by Greenwood and Williamson,[2] from that between Σ_s and W, which holds whatever the (elastic or plastic) regime of deformation of the load-bearing asperities.

The fine variations of the friction coefficient $\mu=F/W$ responsible for the complexities of stick-slip dynamics appear to be very successfully described by the phenomenological state- and rate-dependent friction (SRF) model[3–5] formulated by Rice and Ruina on the basis of Dieterich's experiments on rocks. The SRF model has been, since, extensively validated on very different materials, namely, paper and polymer glasses.[6–8]

The model states that the dynamic friction coefficient depends both on the instantaneous sliding velocity $\dot{x}$ and on a time-dependent state variable ϕ:

$$\mu\equiv\mu(\dot{x},\phi)=\mu_0+B\ln\left(\frac{\phi}{\phi_0}\right)+A\ln\left(\frac{\dot{x}}{V_0}\right). \tag{2}$$

A and B are always measured to be positive and, typically, of order 10^{-2}. It has been suggested that ϕ can be interpreted as the age of the MCI, i.e., as the average time elapsed since the contacts existing at a given instant were first formed. For example, in stationary motion at velocity V, contacts are destroyed and replaced by a noncorrelated set of fresh ones after sliding a length D_0, so that $\phi=D_0/V$. D_0, measured to lie in the micrometer range, compares with microcontact diameters.

More generally, the SRF model describes the time evolution of ϕ by

$$\dot{\phi}=1-\frac{\dot{x}\phi}{D_0}, \tag{3}$$

which interpolates with the static case ($\phi=t$).

In Eq. (2), one then chooses $\phi_0=D_0/V_0$, so that μ_0 is a reference value for steady sliding at some velocity V_0 in the relevant low-velocity range.

The two corrections to μ_0 in Eq. (2) are immediately seen to have different physical contents.

(i) The first one, $B\ln(\phi/\phi_0)$, expresses that contacts strengthen logarithmically with age, as also appears from the logarithmic increase of the static friction coefficient μ_s with waiting time t_s. We have given a detailed proof in a preceding paper,[9] hereafter referred to as (I), that, as already suggested by Dieterich and Kilgore,[10] static aging does result from the increase of the load bearing area Σ_r due to asperity creep under normal compression. In nonsteady motion, $\phi(t)$ [Eq. (3)] keeps track of the previous slip history on the finite distance D_0. So the ϕ-dependent contribution to μ describes a retarded response to velocity variations. In steady sliding, it is *velocity weakening*.

(ii) These characteristics contrast with the instantaneous, *velocity strengthening*, term $A\ln(\dot{x}/V_0)$, usually referred to as describing the ''direct effect'' (since it accounts for the short-time force variation following a jump of the driving velocity[4]).

It is the interplay between these two terms which is responsible for the oscillatory nature of the stick-slip bifurcation, the existence of which indicates that $(B-A)>0$.

While, as mentioned above, the origin of the velocity-weakening term—namely, the slow creep growth of Σ_r—is now clear, the physical content of the direct effect has remained up to now elusive. In terms of Bowden and Tabor's decomposition, it seems natural to interpret it as a weak positive velocity dependence of the interfacial strength σ_s itself. That is, it is likely to carry information about where exactly within the microcontacts shear is accommodated and, possibly, about the size of the dynamical units responsible for dissipation in shear sliding.

The second line of investigation,[11,12] initiated by Yoshizawa and Israelachvili, deals with single microcontacts between atomically flat surfaces with a well-defined geometry. Typical lateral dimensions are in the 1–10 μm range. The (usually mica) flat surfaces are in general separated by a few molecular layers of a highly confined organic lubricant. Under normal stresses of order 10^2 MPa and for short lubricant molecules, a pinned static state and a dissipative sliding one are observed. They are interpreted in terms of solidification (in general in an amorphous state) of the boundary layer under compression and of a shear melting transition.

It is often suggested that such configurations model the microcontacts of a macroscopic MCI. The high local confining pressure would result from the stress-amplifying geometry of the Greenwood interface, while shear would be accommodated within a thin film of contaminants.

To what extent this captures the features of MCI nominally dry friction still remains undecided. Indeed, up to now, such experiments have not been performed over a velocity range large enough to provide a decisive test as regards MCI phenomenology, namely, observation of a velocity-strengthening friction stress compatible with the direct effect of the SRF law.

The present work aims at contributing to bridge these two—macroscopic and microscopic—approaches. For this purpose, we rely upon an extensive experimental study of friction at MCI's between polymer glasses. A previous article (I) has reported the results concerning the time evolution (aging) of the static friction coefficient $\mu_s(t)$ for PMMA and PS (polystyrene) at temperatures ranging from 300 K to their respective glass transition temperatures ($\simeq 400$ K). A summary of these results is given in Sec. II A. We have complemented them with a study of dynamic friction in the same systems, which is reported in Sec. II B.

These experimental results fully confirm the validity of the SRF description. We deduce from them the temperature dependence of the relevant parameters A, B, and D_0. In particular, following the works of Briscoe and Evans[13] on Langmuir-Blodgett layers and of Nakatani[14] on rocks, we analyze the data concerning the coefficient of the direct effect, A, with reference to an underlying thermally activated mechanism. From this, we deduce an activation volume which is of order $(\mathrm{nm})^3$.

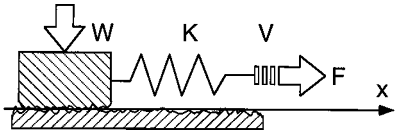

FIG. 1. Schematic representation of the model system. The slider and the track are nominally flat bodies, exhibiting a micron-scale roughness, and forming a multicontact interface (MCI). The slider, loaded by a normal force W, is driven along the track with a remote point velocity V, through a compliant stage of stiffness K.

This leads us to propose (Sec. III) a model of dry friction of a MCI in which the SRF equation [Eq. (2)] is recast into a generalized Tabor expression

$$F=\sigma_s(\dot{x})\Sigma_r(\phi), \tag{4}$$

with

$$\Sigma_r(\phi)=\Sigma_0\left[1+m\ln\left(\frac{\phi V_0}{D_0}\right)\right], \tag{5}$$

$$\sigma_s(\dot{x})=\sigma_{s0}\left[1+\alpha\ln\left(\frac{\dot{x}}{V_0}\right)\right]; \tag{6}$$

that is, drawing upon the results of (I), we associate the age effect with creep growth of the microcontacts. We then show that the direct effect [Eq. (6)] on the interface shear strength can be described in the following frame, previously proposed by Persson:[15] shear localizes within a nanometer-thick layer, forming the junction between contacting asperities. In this layer, sliding proceeds via the shear-induced depinning of bistable ''nanoblocks'' of volume $\sim(\mathrm{nm})^3$, which pave the layer densely. As the contact slides, these blocks—analogous to the two-level centers well known in glasses—are swept up to their spinodal instability, where energy is dissipated in the associated jump, giving rise to friction.[16] These jumps are uncorrelated.

The direct effect ($\dot{x}$ dependence of σ_s) results from the combined effects of sweeping the bistable stress-strain characteristics and of noise-activated premature nanoblock depinning, i.e., thermally activated jumps over the spinodal barrier occurring during the sweep — a mechanism which was already proposed by Larkin and Brazovskii[17] in the framework of charge-density-wave (CDW) transport.

In short, we model the dry friction of macroscopic solids, and interpret the SRF phenomenology for a macroscopic MCI in terms of the elastoplasticity of a highly confined nanometer-thick amorphous layer (the ''joint'') weaker than the bulk of the asperities, which therefore naturally localizes shear.

II. EXPERIMENTAL METHODS AND RESULTS

The tribometer setup has been fully described in (I). Its principle is schematized in Fig. 1. The macroscopic slider and the track, made of the same material, are nominally flat but exhibit a 1.3 μm roughness. The interface is therefore of the MCI type. The control parameters are the weight W of the slider, the driving velocity V, the stiffness K of the driving stage, and the temperature T of the whole system. This latter can be fixed between room temperature (20 °C) and the temperature of the glass transitions of PS ($T_g \cong 102\,°\mathrm{C}$) and PMMA ($T_g \cong 110\,°\mathrm{C}$). The driving velocity ranges between 10^{-1} and $10^{2}\ \mu\mathrm{m\,s^{-1}}$. The applied tangential force is measured through the deflection of the cantilever spring which also imposes the stiffness K of the setup.

A. Static friction results: A summary

Let us first briefly recall the main results reported in (I), concerned with the dependence of the static friction coefficient μ_s on waiting time t_s and temperature T. At fixed T, μ_s is found to increase quasilogarithmically with t_s, over a typical range $1-10^3$ s. We have therefore systematically determined the parameter $\beta_s(T) = \partial\mu_s/\partial \ln t_s$, measured at constant T, for a fixed value V_{load} of the loading point velocity. In addition, two different tangential stress conditions during waiting have been used, namely, (i) zero tangential load and (ii) quasiconstant finite load close to the dynamic friction force at velocity V_{load}.

The corresponding β_s values are denoted $\beta_s^{\varnothing}$ and β_s^{τ}. It was found that, systematically, $\beta_s^{\tau} > \beta_s^{\varnothing}$. Both parameters increase with T, and the T sensitivity strongly increases on approaching T_g.

The results were analyzed according to Bowden and Tabor's decomposition [Eq. (1)]. The real area of contact $\Sigma_r(t_s)$ of our MCI's, which have been found to obey Greenwood's statistical description, is composed of N microcontacts (with N proportional to the normal load W) of average radius $a(t_s)$. Far enough from T_g ($T_g - T \gtrsim 20\,°\mathrm{C}$), the values and T variations of $\beta_s^{\varnothing}$ are successfully described in terms of the increase of a under constant compressive load W/N, following the creep law determined experimentally in uniaxial compressive tests on the bulk materials.

Close to T_g ($T_g - T \lesssim 20\,°\mathrm{C}$), this model underestimates $d\beta_s/dT$, which points towards an increase with waiting time of the average shear strength σ_s of the interface. The value of $d\sigma_s/d(\ln t_s)$ extracted from this analysis increases strongly when approaching T_g; this variation seems compatible with a strengthening of adhesion via chain reptation across the joint.

This picture suggests that the properties of the adhesive joint may not be primarily determined by contaminants, but, rather, by a thin layer made of confined polymeric tails, mechanically weaker than the bulk.

So, in terms of the SRF phenomenology, we conclude, in agreement with Dieterich and Kilgore's suggestion,[10] that, in general, the age effect is due to the creep-induced slow growth of the load-bearing area. The state variable can thus indeed be understood as an average contact age.

However, it should be kept in mind that, in temperature ranges where configurational relaxation within the joint itself becomes active, a corresponding age-dependent increase of the joint strength is to be expected. Such appears to be the case close to T_g for identical vitreous polymers, due to reptation, and, as observed by Nakatani, in feldspathic gouge at $T \cong 800\,°\mathrm{C}$, where sintering healing between grains is at work.[14]

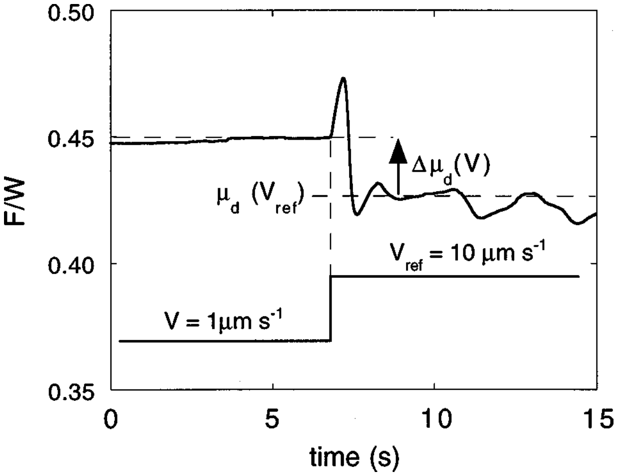

FIG. 2. Response of the system (PS at 20 °C) to a velocity jump within the stable steady sliding region. The effect of the track inhomogeneities is clearly seen at the larger velocity, here V_{ref}.

B. Dynamic friction

We report here the results concerning the sliding dynamics of the same systems at low velocities ranging from 0.1 to $100\ \mu\mathrm{m\,s^{-1}}$.

1. Measurement procedure

In order to remove the long-wavelength variations of the friction force along the track, we proceed as follows. The slider is brought into steady sliding at velocity V by a suitable choice of the control parameters K and W, namely, K/W large enough to prevent the occurrence of stick-slip. The driving velocity is then suddenly jumped to the reference value $V_{ref} = 10\ \ \mu\mathrm{m\,s^{-1}}$. The tangential force is recorded until steady sliding is finally reached again. A typical record is shown in Fig. 2. The friction coefficient difference $\Delta\mu_d(V)$ is computed from the steady state forces: $\Delta\mu_d(V) = [F_d(V) - F_d(V_{ref})]/W$. The average value $\overline{\mu_d(V_{ref})}$ over the track is also measured. The friction coefficients μ_d plotted in Fig. 3 have to be understood as $\mu_d = \overline{\mu_d(V_{ref})} + \Delta\mu_d$. The relative amplitude of the variations of the reference friction coefficient about its mean value at V_{ref} is typically 10%. As clearly evidenced in Fig. 2, the system exhibits velocity weakening, characterized at constant temperature T by the parameter $\beta_d = \partial\Delta\mu_d/\partial \ln V$.

2. Velocity weakening

Logarithmic weakening is generally observed (see Fig. 3), and the data are well fitted by

$$\mu_d(V) = \mu_d(V_{ref}) - \beta_d \ln\frac{V}{V_{ref}}. \tag{7}$$

Close to the glass transition temperature, for both PS and PMMA, however, a trend to saturation of the weakening effect is observed for the highest velocities which the driving stage can impose. The results are found to be correctly described by

$$\mu_d(V) = \mu_{d0} + \beta_d \ln\left(1 + \frac{V_{sat}}{V}\right). \tag{8}$$

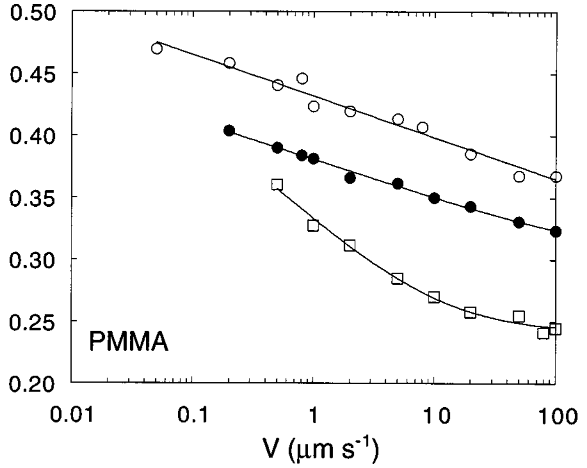

FIG. 3. Experimental data showing velocity weakening of the PMMA-PMMA system at three different temperatures: 23 °C (open circles), 89 °C (solid circles), and 111 °C (squares). The lines are best fits according to Eq. (8). The cutoff velocity at 111 °C is $V_{sat}=11$ μm s^{-1}. The lowest bounds of the velocity ranges correspond to the onset of stick-slip oscillations, which increases with temperature.

The cutoff velocity V_{sat} becomes a relevant fitting parameter, and, in this case, the parameter β_d is measured in the asymptotic part of $\Delta\mu_d(V)$ on the low-velocity side ($V \ll V_{sat}$).

3. Temperature dependence of β_d

PS and PMMA differ markedly as regards the effect of temperature on velocity weakening, as represented in Fig. 4. For PS, at 20 °C, $\beta_d(T)$ is of order 3×10^{-3}. It increases steadily with T. The value at 90 °C is one decade higher than at room temperature. The value of β_d for PMMA at 20 °C is much larger (of order 10^{-2}), but remains quasiconstant over tens of degrees. Its overall increase between room and glass transition temperatures is only twofold. Qualitatively, when compared with the effect of temperature on the aging parameter β_s reported in (I), the temperature sensitivity of velocity weakening appears to be much smaller.

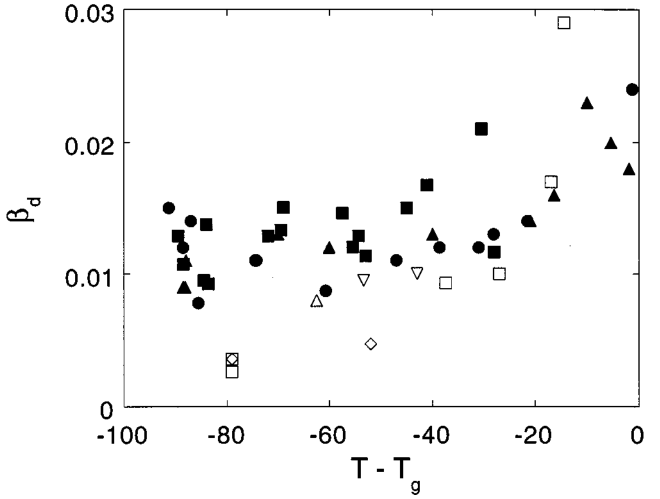

FIG. 4. Velocity weakening parameter β_d vs distance to the glass transition $(T-T_g)$ for PS (open symbols) and PMMA (solid symbols). Different symbol shapes correspond to different samples.

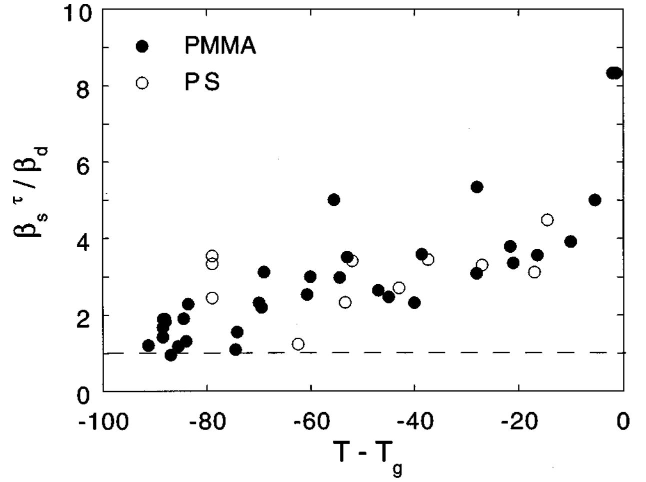

FIG. 5. Ratio of static slope for stressed aging β_s^τ and of dynamic slope β_d vs $(T-T_g)$ for PS and PMMA.

Moreover, β_d is found to be systematically smaller than β_s^τ measured at the same temperature under a tangential load during waiting close below $W\overline{\mu_d}(V_{ref})$, as seen in Fig. 5.

4. Dynamic stability and SRF parameters

The stability of the steady sliding motion of an isothermal spring-slider system against stick-slip oscillations is controlled by the driving velocity V, the stiffness K, and the normal load W. It has been found[6] that K/W is the relevant combination of the latter parameters. It is therefore convenient to seek for the stick-slip bifurcation by tuning W at constant K, V, and T, as illustrated in Fig. 6.

A straightforward linear stability[6] analysis of the SRF equations [Eqs. (2) and (3)] predicts a bifurcation of the di-

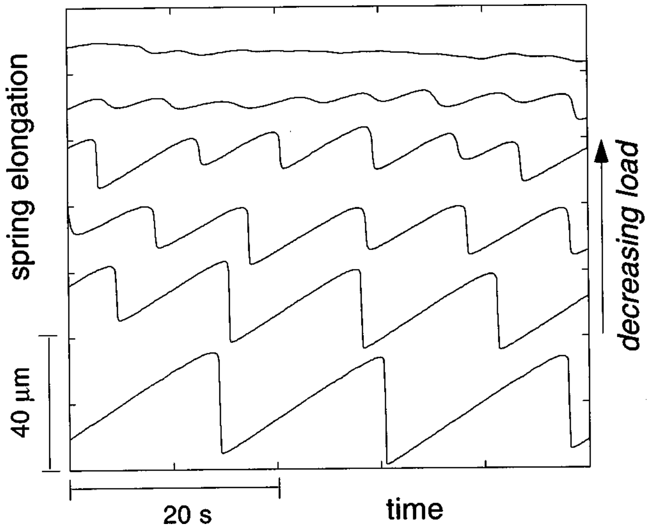

FIG. 6. Bifurcation between stick-slip (lower traces) and steady sliding (upper trace) controlled by the weight W of the slider for a PS-PS interface. W decreases from bottom to top by a total amount of 10 N. Driving point velocity $V=2$ μm s^{-1}, spring stiffness $K=2.1\times10^4$N m^{-1}. Each trace has been shifted upward for the sake of clarity.

rect Hopf type. The critical value $(K/W)_c$ of the driving stage reduced stiffness parameter is such that

$$\chi_c=\left(\frac{K}{W}\right)_c D_0=-\frac{d\mu_d}{d\ln V}=\beta_d. \tag{9}$$

For $(K/W)<(K/W)_c$, stick-slip oscillations occur. Their critical pulsation at the onset of instability is

$$\Omega_c=\frac{V}{D_0}\sqrt{\frac{\chi_c}{A}}. \tag{10}$$

The SRF laws involve three parameters D_0, A, and B with

$$(B-A)=\beta_d. \tag{11}$$

The dynamical analysis provides a simple scheme to determine these parameters;[8] namely, β_d is measured by changing V over decades with a driving stage stiff enough to ensure stable sliding. Its value is then plugged into Eq. (9) to determine D_0 from the measurement of the critical parameter χ_c, and ultimately A is obtained from the critical stick-slip pulsation, according to Eq. (10).

5. Position of the stick-slip bifurcation line

Being essentially interested in the effect of temperature, we have determined the stability limit for a restricted range of velocities, typically 1–10 $\mu\mathrm{m\,s}^{-1}$. We find, in agreement with previous studies,[6,7] that the critical value of K/W decreases slightly with V (see Fig. 6). Increasing T destabilizes markedly the system, therefore leading to a shift of the bifurcation curve towards higher values of K/W. This effect appears clearly in Fig. 7 for both PMMA and PS, while it is more pronounced for the latter glass. It is worth noting that, due to the smallness of $d(K/W)_c/d(\ln V)$, the shift is tremendously amplified when working at constant K/W rather than at constant V.

The destabilizing effect of T is correlated with the increase of the velocity-weakening slope $\beta_d(T)$ which, according to Eq. (9), rules the position of the bifurcation. For a purely logarithmic weakening, the SRF model would predict a V-independent value of the critical parameter χ_c. The slight decrease which is actually measured results from weak nonlinearities of the $\mu_d(\ln V)$ law.[6,7]

6. Memory length D_0

The length D_0 is determined from the knowledge of β_d measured at about 1 $\mu\mathrm{m\,s}^{-1}$. One then computes $D_0=\beta_d(K/W)_c^{-1}$. The results are shown in Fig. 8. The values for PMMA are compatible with a constant value $D_0\simeq 0.5$ μm. Those for PS, also in the μm range, are much more widely scattered and tend to increase with temperature.

7. Direct effect parameter A

The parameter A, characteristic of the rate-dependent term in SRF, Eq. (2), can be determined by different methods.

On the one hand, it can be inferred, using Eq. (10), from the data about the critical pulsation Ω_c at the onset of stick-slip oscillations, together with the previously determined χ_c and D_0. For both PMMA and PS (Fig. 9), $A(T)$ increases markedly with temperature on approaching the glass transition. It has not been possible to approach closer to T_g since in the transition region the system is very unstable and the bifurcation is out of range for the experimental control parameters.

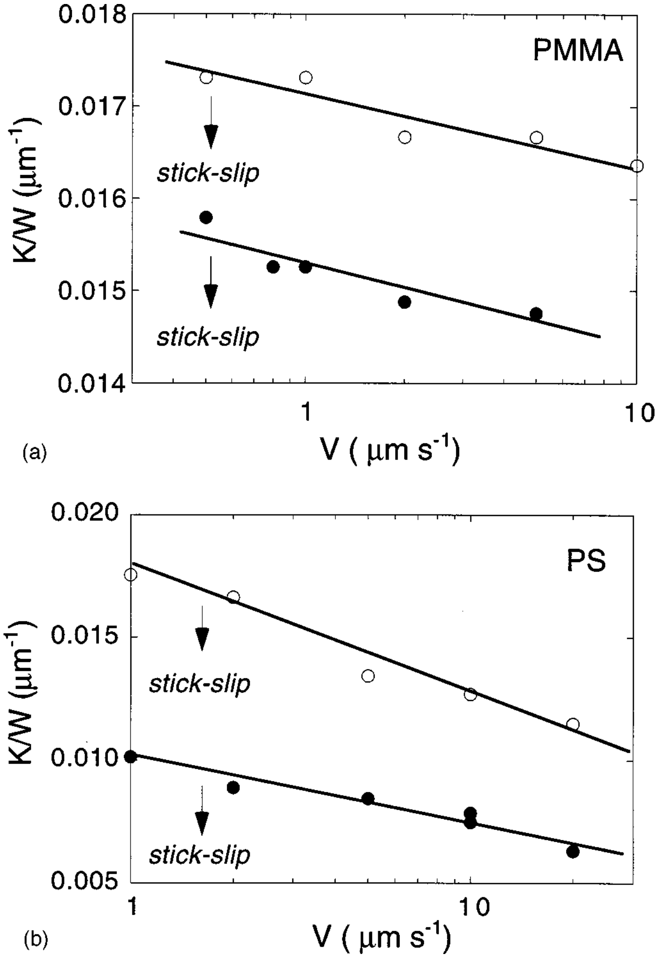

FIG. 7. Stability diagrams in the V-K/W plane for (a) PMMA at $T=24\,°\mathrm{C}$ (solid circles) and 72 °C (open circles); (b) PS at $T=23\,°\mathrm{C}$ (solid circles) and 87 °C (open circles). Below the bifurcation lines the systems exhibit stick-slip oscillations.

On the other hand, A can also be deduced from the tangential force response to a sudden jump of the loading point velocity from V_1 to V_2. As appears clearly in Fig. 2, the tangential force exhibits an initial fast variation. In our low-velocity regime, where inertia is negligible, the velocity of the slider reaches V_2 at the apex of the fast response spike. When loading with a stiff enough spring, this occurs after a time lapse much shorter than the age of the MCI prior to jumping, namely, $\phi_1=D_0/V_1$. In such a case, the age can be safely taken as a constant in Eq. (2), and A is simply related to the spike height $\Delta\mu$ through

$$\Delta\mu=A\ln\left(\frac{V_2}{V_1}\right). \tag{12}$$

The condition for Eq. (12) to hold reads $(\Delta\mu)/(K/V_2)\ll D_0/V_1$, i.e.,

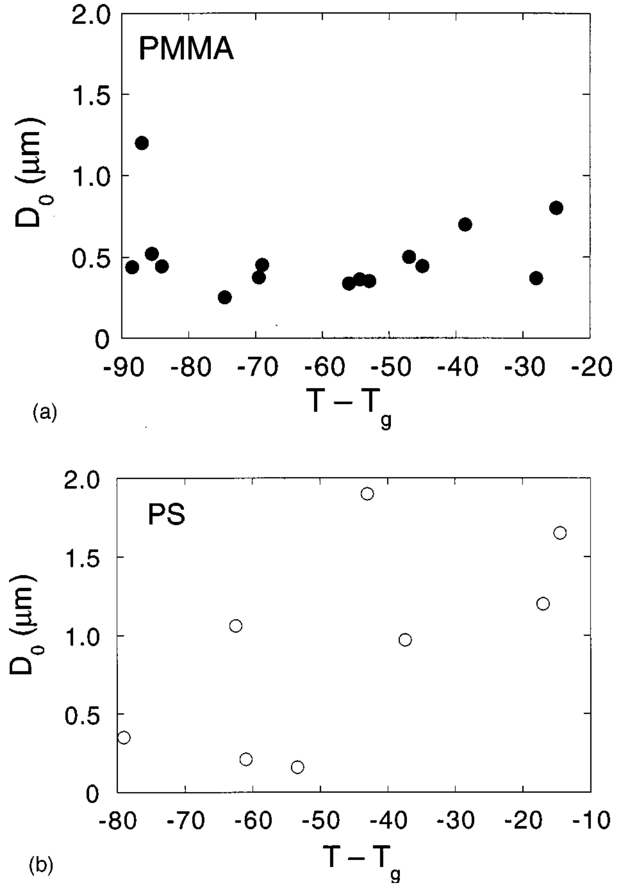

FIG. 8. Memory length D_0 vs temperature for (a) PMMA and (b) PS. Results from different samples are gathered.

$$\frac{KD_0}{W} \gg A\left(\frac{V_1}{V_2}\right)\ln\left(\frac{V_2}{V_1}\right). \qquad (13)$$

This latter requirement becomes more difficult to fulfill as one approches T_g, where A increases significantly. We have measured the force spike $\Delta\mu$ following tenfold velocity jumps (from 1 to 10 $\mu\mathrm{m\,s^{-1}}$) for PMMA. The corresponding values of $A \simeq \Delta\mu/\ln 10$, assuming a constant age, are plotted in Fig. 9. The agreement with those deduced from Eq. (10) is good at room temperature, but deteriorates as T_g is approached. This can be explained by the fact that, the same spring being used at all temperatures, the constant age requirement fails at the highest ones. Indeed, $KD_0/W = 2\times10^{-2}$ is much higher than $A\ln10/10 = 0.23A$ at 20 °C but of comparable order close below T_g, if A is deduced from stick-slip oscillation data.

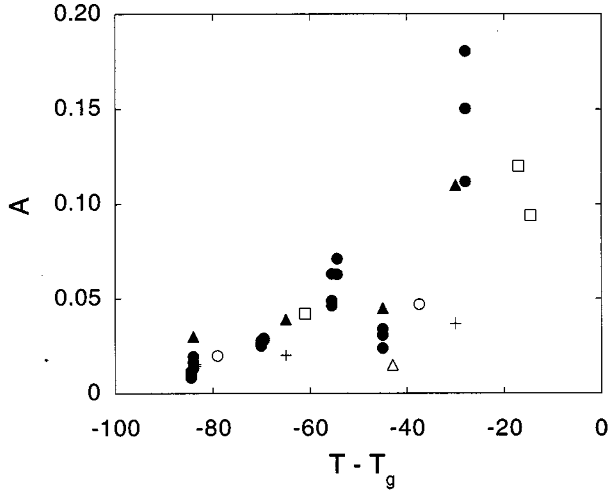

FIG. 9. Direct effect parameter A vs $(T-T_g)$ for PMMA (solid symbols) and PS (open symbols). Different symbols correspond to different samples. The crosses are data obtained from velocity jump experiments on PMMA. See the text for details.

C. Connecting static and dynamic friction

At this stage, we have determined all the SRF parameters, namely, $(B-A)$, A, and D_0.

As expressed by Eq. (2), the SRF expression for μ is singular in the limit of vanishing velocity. We will argue in Sec. III that this limitation does not impair the basic physical content of the SRF approach, but simply results from the fact that the validity of the logarithmic expression for the direct effect should be limited to a finite-velocity bracket.

Intuitively, already at the present stage, given our interpretation of the physics of the aging affect (see Sec. II A above), it appears natural, since, in the static limit, ϕ as defined by Eq. (3) is the waiting time, to state that dynamic aging is essentially equivalent to static aging under a finite tangential stress $\approx W\mu_d(V)$, as far as both processes take place under a combination of normal and tangential loads.

This leads us to compare the SRF parameter B with β_s^τ or, equivalently [see Eq. (11)], the measured values of A and $(\beta_s^\tau - \beta_d)$. Figure 10 shows that, indeed, experimental results support the validity of our interpretation. An analogous conclusion has been also reached recently by Marone[5] for granite.

It has been proposed[4,6] that, in connection with aging, the static and dynamic friction coefficients would be related by a "time-velocity equivalence" relation. Namely, since, for steady sliding at velocity V, $\phi = D_0/V$, they would obey $\mu_d(V) = \mu_s(D_0/V)$, which would entail that $\beta_s = \beta_d$. It is clear from Fig. 5 that this equivalence relation (which is incompatible with the existence of a direct effect contribution to μ_d) does not hold—even though the values of β_s^τ/β_d at room temperature (smaller than 2) and their scatter have misled us into previously claiming its validity.

Another bridge between "static" and dynamic friction can be built, on the basis of the fact that any real measurement of μ_s is performed by loading, from the waiting state, at some finite constant velocity V_{load}. μ_s is then obtained from the peak of the tangential force $F(t)$ at which, when inertia is negligible, since $F(t) = K(V_{load}t - x)$ (see Fig. 1), the instantaneous sliding velocity $\dot{x}_{peak} = V_{load}$.

So μ_s is not, strictly speaking, an intrinsic static property, but a characteristic of a dynamical transient, and can thus be expected to be described by the same SRF expression, Eq. (2), which holds for the sliding dynamics.

Figure 11 shows the variations with waiting time of μ_s^τ, measured on PMMA at $V_{load} = 10$ $\mu\mathrm{m\,s^{-1}}$ and 100 $\mu\mathrm{m\,s^{-1}}$. The aging parameter β_s^τ is found to be independent of V_{load}, while $\Delta\mu = \mu_s^\tau(100\ \mu\mathrm{m\,s^{-1}}) - \mu_s^\tau(10\ \mu\mathrm{m\,s^{-1}}) \cong 7\times10^{-2}$. Since the loading time is always negligible as compared with the waiting time t_s, on the

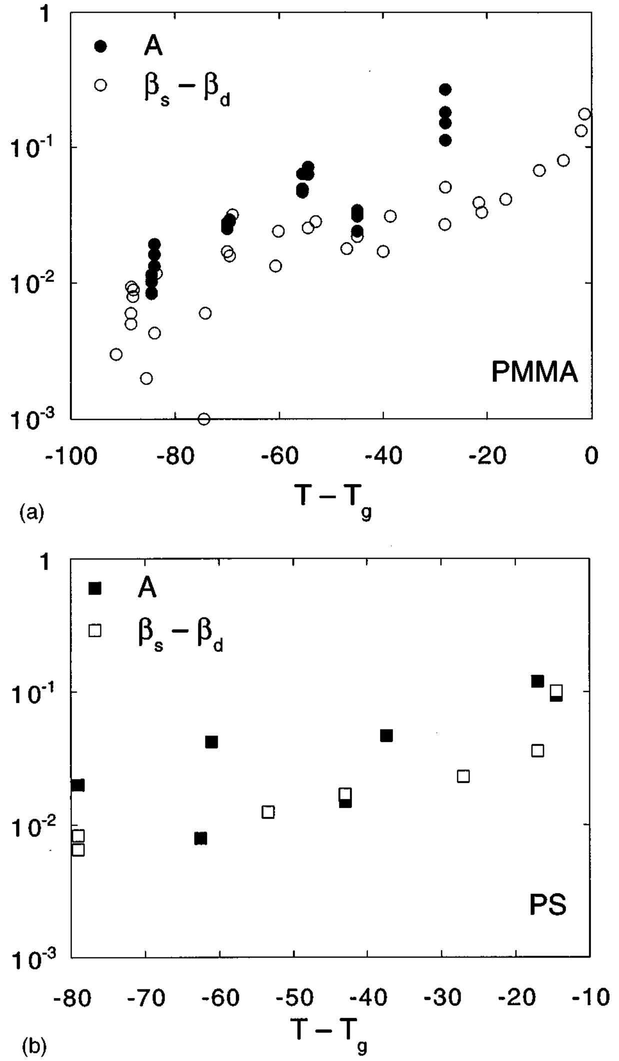

FIG. 10. Comparative plots of parameters A (solid symbols) and $\beta_s^\tau - \beta_d$ (open symbols) vs $(T - T_g)$, for (a) PMMA and (b) PS.

basis of Eq. (2), $\Delta\mu_s$ should result from the direct term only, so that $(\Delta\mu_s/\ln 10)$ should be compared with A which, at this temperature, is found (Fig. 9) to be on the order of $4\times10^{-2}\pm10^{-2}$. This lends further support to the SRF phenomenology: the fact that the direct effect term depends on the instantaneous sliding velocity appears to be reasonably well verified even in the present case, where μ_s is measured during an accelerated transient.

III. DISCUSSION AND MODEL

A. Estimate of an activation volume for shear creep

We have shown in Sec. II C above that the coefficient B of the ''state-dependent'' term in Eq. (2) can be identified with the logarithmic slope β_s^τ of the static friction coefficient $\mu_s^\tau(t_s)$. This enables us to attribute the velocity-weakening contribution to the steady state μ_d to the creep-induced growth of the load bearing area and, consequently, to rewrite the SRF equation [Eq. (2)] as

$$\mu(\dot{x},\phi) = \mu_0\left[1 + m\ln\left(\frac{\phi V_0}{D_0}\right)\right]\left[1 + \alpha\ln\left(\frac{\dot{x}}{V_0}\right)\right], \qquad (14)$$

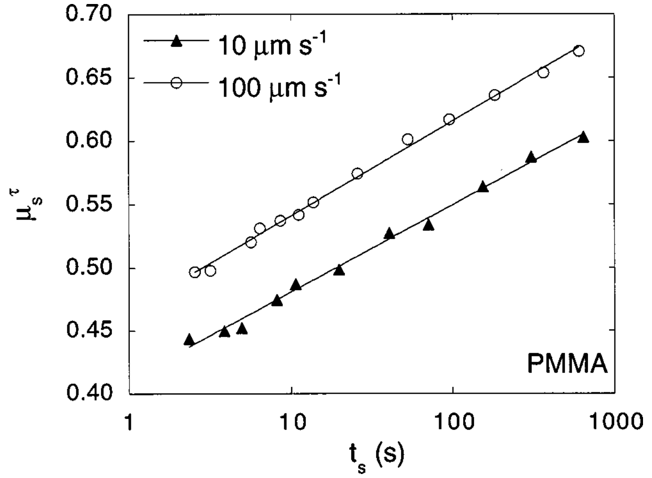

FIG. 11. Static friction coefficients μ_s^τ vs waiting time t_s under tangential load, for loading velocities $V_{load} = 10\ \mu\mathrm{m\,s^{-1}}$ (open circles) and $100\ \mu\mathrm{m\,s^{-1}}$ (solid circles). Note that the logarithmic slope β_s^τ is independent of V_{load}.

$$\mu_0 = \frac{\Sigma_{r0}\sigma_{s0}}{W}. \qquad (15)$$

Σ_{r0} is the real area of contact and σ_{s0} the shear strength in steady sliding at the reference velocity V_0 ($\sim W$ for our Greenwood interfaces). We thus identify

$$A = \alpha\mu_0, \quad B = m\mu_0. \qquad (16)$$

With $V_0 = 1\ \mu\mathrm{m\,s^{-1}}$, μ_0 is typically of order 0.5; hence α and m are on the order of 10^{-1}, so that the second order correction $\mu_0\alpha m(\ln)^2$ spuriously introduced when factoring Eq. (2) into Eq. (14) is of order 5×10^{-3}. This is a small correction, which is precisely comparable in magnitude with the weak nonlinearities of the $\mu_d(V)$ law, neglected by the SRF model, but revealed by the detailed analysis of stick and slip and relaxation.

Equation (14) thus leads us to the generalized Tabor decomposition [Eqs. (4)–(6)] which attributes the direct effect to an interfacial shear strength fitted by the empirical expression [Eq. (6)], which we rewrite here for convenience,

$$\sigma_s(\dot{x}) = \sigma_{s0}\left[1 + \alpha\ln\left(\frac{\dot{x}}{V_0}\right)\right]. \qquad (17)$$

When considering Eq. (17) from the point of view of continuum mechanics, one is naturally prone to associate, following Briscoe and Evans[13] and Bréchet and Estrin,[18] the displacement rate $\dot{x}$ with a shear strain rate $\dot{\epsilon} = \dot{x}/h$, where h is some thickness characterizing an interfacial zone where shear localizes. This interpretation strongly suggests that the logarithmic ''rheology'' expressed by Eq. (17) might result from a thermally activated shear-induced creep process. If such is the case, as shown in Ref. 13, α should read

$$\alpha = \frac{k_B T}{\sigma_{s0} v_{act}}, \qquad (18)$$

which defines the volume v_{act} associated with the elementary dynamical process. With the help of Eq. (16), we get

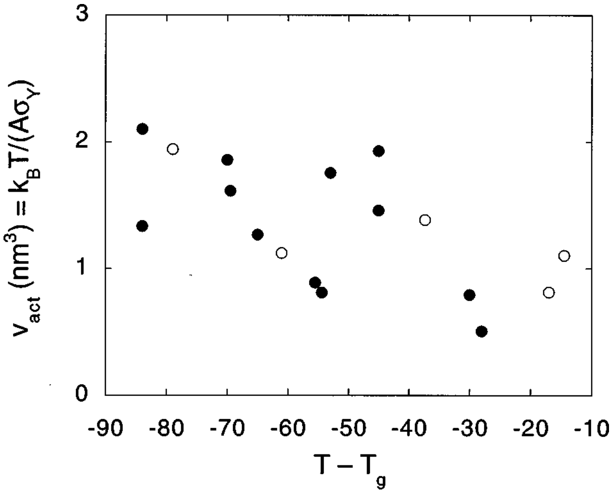

FIG. 12. Activation volume v_{act} associated with the direct effect, as estimated from Eq. (19), vs $(T-T_g)$, for PMMA (solid circles) and PS (open circles).

$$v_{act}=\frac{k_BT}{p}\frac{1}{A}, \tag{19}$$

where the average normal stress acting upon the microcontacts $p=W/\Sigma_{r0}$ is roughly[19] of the order of the yield stress σ_Y of the bulk material in uniaxial compression.

Figure 12 shows the temperature dependence of v_{act}, as deduced from the data of Fig. 9 and from the values of $\sigma_Y(T)$ obtained in (I).

It is seen that, for both PMMA and PS,

$$v_{act}\sim 1\text{–}2\ (\text{nm})^3 \tag{20}$$

and this over the whole temperature range. This indicates that the elementary units of the dissipative dynamics contain a few molecular (sub)units—a size typical of the localized defects (two-level centers) responsible for the plasticity of glassy materials.[20]

B. Origin of pinning and shear localization

In order to get insight into the origin of the direct effect, it is necessary to figure out first where shear localizes. For this purpose, it is essential to recall that two of us[21] have evidenced experimentally the existence, for our MCI's, of a regime of elastic response to tangential loading, which is reversible at low load and crosses over to the dissipative sliding regime in the immediate vicinity of μ_sW (or, equivalently, for displacements $\sim D_0$).

This gives direct proof that the static interface is *pinned* up to a finite threshold stress. In this situation, it is well known that the resulting low-velocity friction force F is due to the stress-induced depinning of multistable states which dissipate a finite energy during the corresponding fast spinodal jumps.[16] The corresponding F is basically velocity independent.

The question then arises of the origin of this multistable pinning. There are *a priori* two possible candidate mechanisms. One is the elastic potential arising from vertical elastic compression during asperity crossing; a simple order of magnitude estimate[22] shows that realistic asperity profiles are much too smooth for compressive pinning to give rise to multistability.

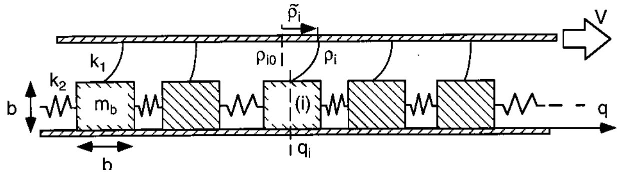

FIG. 13. Schematic representation of Persson's nanoblock model (see Ref. 15) of the adhesive joint between two load-bearing asperities.

The natural candidate is therefore adhesion—a mechanism which we expect to act on, typically, a nanometric thickness range. Adhesive pinning is indeed observed on boundary lubricated single microcontacts,[23] and was also measured long ago by Courtney-Pratt[24] with a dry metallic single contact. For our MCI's, one can reasonably guess that the nanometric interfacial layer in which adhesive interactions are active is essentially constituted of highly confined tails of polymer molecules forming an amorphous "joint." This interfacial layer is certainly less dense or, at least, mechanically weaker than the bulk material, as indicated by the marked decrease of T_g with thickness for very thin PMMA films.[25] This leads us to postulate that it is in this layer that the dissipative processes take place. Moreover, our above estimate of an activation volume points to nanometric lateral dimensions for these units, comparable with the layer thickness.

Persson[15] has proposed a schematic model which displays the essential features of the above qualitative picture. We will therefore now try to interpret our results in the frame of this "nanoblock" model. We first briefly summarize its ingredients, assumptions, and main results.

C. Persson's nanoblock model

The single microcontact is schematized as follows (Fig. 13).

(i) The joint, of lateral extension a, is represented as a linear array of nanoblocks of size $b\times b\times b$, coupled to their nearest neighbors by springs of stiffness $k_2\sim E_Jb$, where E_J is an elastic modulus of the joint. The blocks are coupled elastically to a driving upper plate by shear springs of stiffness $k_1\sim k_2$.

(ii) Each block (i), of abscissa q_i, moves according to the following rules.

(a) As long as the magnitude of the stress $|\sigma_i|$ acting on (i) is smaller than a threshold σ_a, the block is rigidly pinned to the lower rigid nonmoving plate: $\dot{q}_i=0$.

(b) When $|\sigma_i|\geqslant\sigma_a$, it is depinned, and moves, at low driving velocity $\dot{x}$, according to

$$m_b\ddot{q}_i+m_b\gamma\dot{q}_i=k_2(q_{i+1}-2q_i+q_{i-1})+k_1(\rho_i-q_i), \tag{21}$$

where m_b is the block mass, γ the internal viscosity of the joint, and ρ_i the position of the driving point relative to (i).

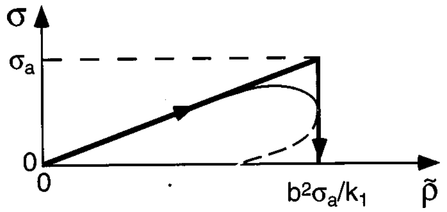

FIG. 14. Stress-driving point displacement characteristics. $\tilde{\rho}$ measures the driving point displacement from its position at the last repinning event. The triangular shape (thick line) approximates a schematic real multistability cycle (thin line).

(c) When $\dot{q}_i$ vanishes for the first time, (i) is repinned (stops), and the process starts again. Note that such a rule implies that the block dynamics is overdamped.[26]

The assumption of complete immobility for $|\sigma_i|<\sigma_a$ is a simplified representation of the pinning of blocks by molecular scale modulations of the ''plate'' potentials. It is the competition between these modulations and the elastic restoring spring forces which, for large enough ρ_i, leads to the spinodal instability at σ_a.

The most serious assumption of the model is the infinite stiffness of the confining plates. This amounts to neglecting elastic deformations of the asperity bodies (represented by the plates) on scales smaller than the contact radius with respect to those of the joint. So it implies that

$$E \gg E_J, \tag{22}$$

where E is an elastic modulus of the bulk material.[27]

If this would not hold, interblock long-range elastic couplings mediated by the body of the asperities would become relevant, thus invalidating the nearest-neighbor coupling assumption.[22] It would then also become crucial to take into account the full (2+1)-dimensional geometry of the elastic system.

Persson has studied this model numerically, and concluded the following.

(i) At driving velocities much smaller than the sound velocity in the joint, $c_J \sim (E_J b^3/m_b)^{1/2}$, a range relevant to our experiments, the steady sliding friction force is V independent.

(ii) The blocks slide essentially independently and in a noncorrelated fashion (only a very small fraction is unpinned at a given time).

(iii) Accordingly, the distribution function $P(\sigma)$ of single-block stresses is stationary and V independent. It is, very roughly, uniform between $\sigma_{min}\approx 0$ and $\sigma_{max}=\sigma_a$, with $P(\sigma_a)\neq 0$.

These results can be reinterpreted, for semiquantitative purposes, in terms of the following mean field picture: When sliding, each block is swept across a stress-driving point displacement characteristics $\sigma(\tilde{\rho})$, ending abruptly at the spinodal limit σ_a (Fig. 14). Here, $\tilde{\rho}_i=\rho_i-\rho_{i0}$, where ρ_{i0} is the position of the ith driving point at the instant when block i was repinned for the last time. In mean field, variations of σ_i and ρ_i for pinned blocks are related by $\delta\sigma_i=k_1\delta\rho_i/b^2$, for each block $\sigma_i=\sigma(\tilde{\rho}_i)$, and the block reference coordinates $\tilde{\rho}_i$ have a uniform distribution $Q(\tilde{\rho})$. The frictional stress on a microcontact is

$$\overline{\sigma_s}=\int_0^{\sigma_a}\sigma P(\sigma)\,d\sigma, \tag{23}$$

with $P(\sigma)=\sigma_a^{-1}$, so that $\overline{\sigma_s}=\sigma_a/2$.

Note that, in this highly simplified picture, the stress-displacement hysteresis cycle is made of two strictly linear curves interrupted at $\pm\sigma_a$. The absence of the (generic) infinite $(d\sigma/d\rho)$ slope at the spinodal limit results from neglecting elastic displacements within the molecular block-pinning potential wells.

D. Thermally activated premature depinning

The previous results are concerned with the zero-temperature limit. At finite T, thermal noise is necessarily present. When swept by the driving plate along the stress cycle, a block is pinned in a locally stable state whose energy increases with σ, so that it gradually evolves from globally stable to metastable, until it disappears at σ_a, via a saddle-node bifurcation. That is, as $\tilde{\rho}$ approaches the spinodal limit $\tilde{\rho}_{max}$ from below, the energy barrier $\Delta U(\tilde{\rho})$ which separates the pinned equilibrium state from the depinned one gradually decreases to zero.

In the absence of externally imposed drift, metastable blocks with reference coordinate $\tilde{\rho}$ would escape, due to thermal noise, above the activation barrier $\Delta U(\tilde{\rho})$, at the rate

$$\frac{1}{\tau(\tilde{\rho})}\approx\omega_a \exp\left[-\frac{\Delta U(\tilde{\rho})}{k_B T}\right], \tag{24}$$

where the attempt frequency $\omega_a \approx c_J/b$. In this situation (which corresponds to the static state of the interface under a load $\sim\mu_d W$), the rightmost part of $Q(\tilde{\rho})$ gets gradually depleted by these premature depinning events, which are all the more effective that $\tilde{\rho}$ is closer to $\tilde{\rho}_{max}$: and the average stress on the microcontact decreases, the slider *creeps under shear*.

When the joint is driven at the fixed velocity $\dot{x}=V$, each block is at the same time advected towards larger $\tilde{\rho}$ and experiencing the above finite $\tilde{\rho}$-dependent depinning probability. The larger V, the less time a block spends in the vicinity of the spinodal, where the escape rate is non-negligible. The corresponding distribution $Q(\tilde{\rho})$ is, consequently, strongly depleted above a cutoff $\tilde{\rho}_c(V)$ which increases with V. The average frictional stress increases accordingly. At large velocities, advection overrides activation. Q (and, equivalently, P) recovers its uniform $T=0$ value, and σ_s saturates at $\overline{\sigma_s}$.

This picture can be formalized by writing the evolution equation for $Q(\tilde{\rho})$, which reads

$$\frac{\partial Q}{\partial t}=-V\frac{\partial Q}{\partial\tilde{\rho}}-\frac{Q}{\tau(\tilde{\rho})}, \tag{25}$$

with the boundary condition

$$Q(\tilde{\rho}_{min},t)=Q(\tilde{\rho}_{max},t)+\int d\tilde{\rho}'\,\frac{Q(\tilde{\rho}',t)}{\tau(\tilde{\rho}')}, \tag{26}$$

which expresses that the depinned blocks refeed the lower edge of the distribution.

The steady state distribution reads

$$Q_{st}(\tilde{\rho},V)=Q_0\exp\left[-\int_0^{\tilde{\rho}}\frac{d\tilde{\rho}'}{V\tau(\tilde{\rho}')}\right] \tag{27}$$

and the average frictional stress

$$\sigma_s(V)=\int_0^{\sigma_a}\sigma Q_{st}(\tilde{\rho}(\sigma),V)\frac{d\tilde{\rho}}{d\sigma}d\sigma, \tag{28}$$

with $(d\tilde{\rho}/d\sigma)=(b^2/k_1)$.

For velocities $V \ll V^* = c_J(k_BT/\sigma_a b^3)$, Q_{st} [Eq. (27)] can be shown[16] to exhibit a very abrupt drop from its $T=0$ value to practically complete depletion about a cutoff $\tilde{\rho}_c(V)$ defined by

$$\tau_c \equiv \tau(\tilde{\rho}_c)=\frac{k_BT}{V|(d\Delta U/d\tilde{\rho})_{\tilde{\rho}_c}|}. \tag{29}$$

One then obtains[15]

$$\sigma_s(V)=\bar{\sigma}_s\left[1+\frac{k_BT}{\bar{\sigma}_s b^3}\frac{E_J}{8\bar{\sigma}_s}\ln\left(\frac{V}{V^*}\right)\right]. \tag{30}$$

When introducing, in the spirit of Sec. II, a reference velocity V_0, Eq. (30) reduces to the direct effect expression, Eq. (17), with

$$\sigma_{s0}=\bar{\sigma}_s\left[1-\frac{k_BT}{\bar{\sigma}_s b^3}\frac{E_J}{8\bar{\sigma}_s}\ln\left(\frac{V^*}{V_0}\right)\right], \tag{31}$$

$$\alpha=\frac{k_BT}{\bar{\sigma}_{s0}b^3}\frac{E_J}{8\bar{\sigma}_s}. \tag{32}$$

This is to be compared with the expression of α [Eq. (18)], which we used to evaluate an effective activation volume v_{act}. From Eq. (32), this is related to the joint parameters and block volume by

$$v_{act}=b^3\frac{8\bar{\sigma}_s}{E_J}. \tag{33}$$

For shear melting of confined boundary layers, Thompson and Robbins[28] suggest that, roughly, $\bar{\sigma}_s/E_J \approx 5\times 10^{-2}$. With this evaluation and the value of v_{act} extracted from experiments, we do obtain values of the block size b in the nanometer range.

So not only does the above model account for the functional form of the direct effect V dependence of the interfacial strength, but it appears quantitatively consistent.

It is important to point out that, while the detailed values of the coefficients σ_{s0} and α in Eqs. (31) and (32) result from the particularly simple choice of a linear truncated stress-displacement block characteristic, the logarithmic V dependence of σ_s in Eq. (30) is robust. Indeed, it results directly from the exponential dependence of the rate $[1/\tau(\tilde{\rho})]$ of activated premature depinning. Departures from this behavior are to be expected only at velocities large enough for $\tilde{\rho}_c(V)$ to lie in the close vicinity of $\tilde{\rho}_{max}$ where the generic infinite $(d\sigma/d\tilde{\rho})$ slope at the spinodal limit will result in a slower $[\ln(V/V^*)]^{2/3}$ variation[16] of $[\sigma_s(V)-\bar{\sigma}_s]$ which, at even higher V, far above our experimental range, finally crosses over to the ''phonon drag'' regime where dissipation is controlled by the internal viscosity γ. Since the reduced velocity relevant to viscous dissipation is V/c_J, the crossover region is very wide, and corresponds to an apparent saturation of the frictional stress at the constant value $\bar{\sigma}_s$.

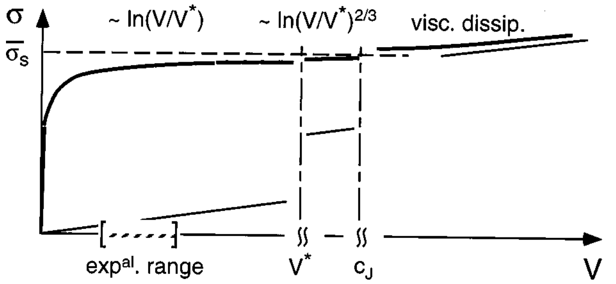

FIG. 15. Schematic interfacial stress vs velocity curve (thick line). Note the breaks on the velocity axis (see text). The thin line corresponds to the asymptotic (Newtonian) viscous regime, controlled by the internal viscosity γ.

Another crossover is expected on the low-velocity side. Indeed, as the stress decreases, $\tilde{\rho}_c(V)$ approaches from above the position corresponding to the Maxwell plateau[16] and repinning backjumps, though extremely rare, become almost as frequent as depinning ones. This results in the classical Eyring (sinh) behavior for $\sigma_s(V)$ ending in an extremely fast quasilinear drop extrapolating to zero.

These behaviors are schematically summarized in Fig. 15.

E. Activated depinning for nonsteady motion

Finally, in order to ascertain that activated premature depinning fully accounts for the SRF expression, Eq. (6), we must extend Eq. (30), which holds for steady sliding only, to the case of accelerated motion with velocity $\dot{x}(t)$.

The equation for $Q(\tilde{\rho},t)$ retains its form [Eq. (25)], with $V \rightarrow \dot{x}(t)$. One expects that, for slow enough velocity variations, the system adapts adiabatically to the instantaneous $\dot{x}$, i.e., that

$$Q(\tilde{\rho},t)\approx Q_{st}(\tilde{\rho},\dot{x}(t)). \tag{34}$$

One easily checks that this $(\partial Q/\partial t \ll Q/\tau)$ holds as long as

$$\frac{\ddot{x}}{\dot{x}} \ll \frac{1}{\tau(\tilde{\rho})}\left[\int_0^{\tilde{\rho}}\frac{d\tilde{\rho}'}{\dot{x}\tau(\tilde{\rho}')}\right]^{-1}. \tag{35}$$

One shows[16] that the above integral is of order $(k_BT)/[\dot{x}\tau(\tilde{\rho})|\Delta U'(\tilde{\rho})|]$. Finally, as can be intuitively expected, the condition of adiabatic adaptation reduces to

$$t^* \gg \tau_c(\dot{x}), \tag{36}$$

where t^* is the time scale of velocity variations, and $\tau_c(\dot{x})$ is the activation time corresponding to the upper cutoff of Q_{st} at velocity $\dot{x}$ [Eq. (29)]. Plugging Persson's expression for the activation barrier height,

$$\Delta U(\sigma)=\sigma_a b^3 \frac{\sigma_a}{E_J}\left(1-\frac{\sigma^2}{\sigma_a^2}\right), \qquad (37)$$

into Eq. (29), we find that condition (36) yields

$$t^* \gg t_a(\dot{x}) = \frac{b}{\dot{x}}\,\frac{k_B T}{4\overline{\sigma}_s b^3}. \qquad (38)$$

For $\dot{x}\approx 1$ μm s^{-1}, $b\sim 1$ nm, and $k_BT/\overline{\sigma}_s b^3 \approx A$ (the SRF parameter), we obtain $t_a(\dot{x})\sim 10^{-5}$ s.

This is to be compared with the time scales relevant to, essentially, three types of experimental situations.

(i) Stick-slip oscillations: close to the bifurcation, t^* is the inverse of the critical frequency Ω_c [Eq. (10)], i.e., of order $2\pi D_0/V_{drive}$. So $t^*/t_a(\dot{x})\approx D_0/bA\sim 10^5$.

Far from the bifurcation, t^* is governed by the time for inertial slip: $t_{in}\sim\sqrt{M/K}$, where M is the slider mass and K the stiffness of the driving spring. Typically, since $(K/M) < (K/M)_c$, $t_{in} > 10^{-3}$ s.

(ii) When measuring the dependence of μ_s on V_{load} (Sec. II C) one deals with the acceleration of the slider from $\dot{x} \simeq 0$ to $\dot{x}=V_{load}$ within a time $t^*\gtrsim D_0/V_{load}$,[29] to be compared with $t_a(V_{load})$. Hence, again, $t^*/t_a(V_{load})\sim 10^5$.

(iii) Velocity jumps from V_1 to $V_2>V_1$: t^* is the time needed to increase the load, at velocity V_2, by $AW\ln(V_2/V_1)$, to be compared with $t_a\approx bA/V_2$. Steady sliding requires $\chi = KD_0/W > \chi_c = \beta_d \sim 10^{-2}$. Typically in the experiments, $\chi/\chi_c<10$. Hence $t^*/t_a=(\chi^{-1}D_0/b)\ln(V_2/V_1)\sim 10^4$.

From this we conclude that, in all dynamical situations relevant to low driving velocities, it is legitimate to extend Eq. (30) to nonsteady motion by simply replacing V by the instantaneous slider velocity. This completes our interpretation of the direct SRF effect in terms of the competition between activated depinning and sweeping of multistable characteristics of nanoblocks.

IV. CONCLUSION

In summary, the quantitative analysis of our experiments on static and dynamic friction leads us to conclude that, for our MCI's between polymer glasses at least, the SRF model provides an excellent phenomenological description of the frictional dynamics. It can legitimately be interpreted physically in terms of a generalized Bowden-Tabor decomposition of the friction force.

The SRF, contact-strengthening (V-weakening), age effect results from the slow creep of asperity microcontacts under normal compression, leading to logarithmic growth of the real area of contact.

The velocity-strengthening ''direct effect'' SRF contribution to μ is attributable to the premature depinning, due to thermal noise, of a two-dimensional layer of elementary dynamical units of nanometric dimensions, forming what we call the adhesive joint. Frictional sliding corresponds to sweeping these nanoblocks up to a spinodal instability where they flip back into a relaxed stress state. Such a description is akin to the model of plasticity of amorphous solids recently proposed by Falk and Langer.[30] These (uncorrelated) jumps are responsible for the finite V-independent dynamic friction force, to which the activated direct term appears as a small logarithmic correction.

We therefore interpret friction in terms of the plastic deformation of elastoplastic adhesive joints, much weaker mechanically than the bulk materials, driven by the bodies of the (adjacent) load-bearing asperities, to which they are elastically pinned when unsheared.

In this model the whole dissipation takes place in the joint. Bréchet and Estrin[18] have suggested that it might, on the contrary, result from plastic creep within the asperity bodies. However, their model implicitly assumed infinitely strong adhesive pinning. In the real case where, as proved by the existence of a finite memory length D_0, the interfacial strength $\overline{\sigma}_s$ is finite, the effect of asperity creep can be estimated as follows. When the joint slides, the friction stress is approximately $\overline{\sigma}_s$. Hence a rate of plastic deformation in the asperities: $\dot{\epsilon}_{pl}(\overline{\sigma}_s)$. The velocity at which the joint is driven is therefore $v_J\approx[V-\dot{\epsilon}_{pl}(\overline{\sigma}_s)a]$, with a the contact diameter. As long as $v_J>0$, the joint is effectively sliding. The total dissipation, controlled by $\overline{\sigma}_s$, is unaffected by asperity creep whose only effect is that dissipation is now redistributed between two contributions associated, respectively, with joints and asperities. It is only at velocities $V<V_{plast}=a\dot{\epsilon}_{pl}(\overline{\sigma}_s)$ that the joint remains pinned while the asperity flows plastically in a chewing-gum-like fashion. Then $\sigma_s(V) = (\dot{\epsilon}_{pl})^{-1}(V/a)$. Since the asperities are stronger than the bulk, $\overline{\sigma}_s$ is much smaller than the yield stress of the asperities, so that the Bréchet-Estrin regime is, in general, restricted to extremely small velocities, irrelevant to our experiments.

Let us insist again that Persson's model which is the basis of our interpretation, as well as the mean field approximation to which it is amenable, depends crucially on the validity of condition (22) which states that the joint be much more compliant than the bulk material. For systems where this condition is not satisfied, long-range elastic interactions between nanoblocks, mediated by the asperity bodies, become relevant. These will certainly promote correlations between block flips, which might result, for example, in kinklike compression waves or possibly decohesion waves of the Schallamach type. This suggests that it should be of interest to perform systematic friction studies on multicontact systems involving ''soft'' materials.

Note finally that our interpretation provides support to the classical Mindlin model of a sheared adhesive Hertz contact.[31] Indeed, this continuum mechanics description relies upon the concept of a *local* Amontons-Coulomb law with a constant friction coefficient. Such a law necessarily results from an averaging, which should be valid on a scale much smaller than the (micrometric) asperity diameter. This is indeed justified if, as we concluded above, the basic dynamical units are of nanometric size. Of course, even if the averaging process on this scale is legitimate, it remains to be proved that the Amontons-Coulomb proportionality holds between local shear and normal stresses. A recent simulation[32] by He *et al.* of a sheared confined boundary layer indicates that such a linear relationship is indeed to be expected.

This, however, does not permit us to justify the use of a *local* version of the SRF model. Indeed, the ''state'' variable ϕ is an *average* contact age. Such an average can only be defined on a scale much larger than the mean intercontact distance. It is meaningful only on a semimacroscopic scale.

ACKNOWLEDGMENTS

We are grateful to B. Velicky for fruitful discussions and to O. Ronsin for a critical reading of the manuscript.

---

[*] Present address: Groupe de Physique du Solide, 2 place Jussieu, 75251 Paris Cedex 05, France.

[†] Present address: INRA, Unite d'Agronomie de Laon-Peronne, rue Fernand-Christ, 02007 Laon Cedex, France.

[‡] ''Associé au Centre National de la Recherche Scientifique et aux Universités Paris 6 et Paris 7.''

[1] F. P. Bowden and D. Tabor, *The Friction and Lubrication of Solids* (Clarendon, Oxford, 1950).

[2] J. A. Greenwood and J. B. P. Williamson, Proc. R. Soc. London, Ser. A **295**, 300 (1966).

[3] J. R. Rice and A. L. Ruina, J. Appl. Mech. **105**, 343 (1983).

[4] See, e.g., C. H. Scholtz, *The Mechanics of Earthquakes and Faulting* (Cambridge University Press, Cambridge, England, 1990), Chap. 2.

[5] For a recent review, see C. Marone, Annu. Rev. Earth Planet Sci. **26**, 643 (1998), and references therein.

[6] F. Heslot, T. Baumberger, B. Perrin, B. Caroli, and C. Caroli, Phys. Rev. E **49**, 4973 (1994).

[7] T. Baumberger, C. Caroli, B. Perrin, and O. Ronsin, Phys. Rev. E **51**, 4005 (1995).

[8] See, e.g., T. Baumberger, Solid State Commun. **102**, 175 (1997).

[9] P. Berthoud, T. Baumberger, C. G'Sell, and J.-M. Hiver, Phys. Rev. B **59**, 14 313 (1999).

[10] J. H. Dieterich and D. Kilgore, Pure Appl. Geophys. **43**, 283 (1984).

[11] H. Yoshizawa and J. Israelachvili, J. Phys. Chem. **97**, 11 300 (1993).

[12] See, e.g., MRS Bull. **18** (1993).

[13] B. J. Briscoe and D. C. B. Evans, Proc. R. Soc. London, Ser. A **380**, 389 (1982).

[14] M. Nakatani, Ph.D. thesis, University of Tokyo, 1997.

[15] B. N. J. Persson, *The Physics of Sliding Friction* (Springer, Heidelberg, 1998) and references therein.

[16] C. Caroli and P. Nozières, in *Physics of Sliding Friction*, edited by B. N. J. Persson and E. Tosatti, Vol. 311 of *NATO Advanced Study Institute, Series E: Applied Sciences* (Kluwer, Dordrecht, 1996), p. 27.

[17] A. Larkin and S. Brazovskii, Solid State Commun. **93**, 275 (1995).

[18] Y. Bréchet and Y. Estrin, Scr. Metall. Mater. **30**, 1449 (1994).

[19] The Greenwood plasticity indices of our MCI's are estimated [see (I)] to be of order 1.

[20] P. H. Mott, A. S. Argon, and U. W. Sutter, Philos. Mag. A **67**, 931 (1993).

[21] P. Berthoud and T. Baumberger, Proc. R. Soc. London, Ser. A **454**, 1615 (1998).

[22] C. Caroli and P. Nozière, Eur. Phys. J. B **4**, 233 (1998).

[23] G. Reiter, A. Levent Demirel, J. Peanasky, L. L. Cai, and S. Granick, J. Chem. Phys. **101**, 2606 (1994).

[24] F. P. Bowden and D. Tabor, *The Friction and Lubrication of Solids* (Clarendon, Oxford, 1964), Pt. II.

[25] J. A. Forrest, C. Svanberg, K. Révész, M. Rodahl, L. M. Torell, and B. Kasemo, Phys. Rev. E **58**, R1226 (1998), and references therein.

[26] T. Baumberger and C. Caroli, Eur. Phys. J. B **4**, 13 (1998).

[27] Note that, even when Eq. (21) holds, the interface elastic stiffness of the MCI's remains in general governed by the asperity one ($K_{asp} \sim Ea$), which must be compared with the joint stiffness $K_J \sim E_J a^2/D \sim K_{asp}(E_J/E)(D/a)$, with $D/a \approx 10^{-3}$.

[28] P. A. Thompson and M. O. Robbins, Science **25**, 792 (1990).

[29] The acceleration is therefore $\ddot{x} \lesssim V_{load}^2/D_0$. For $V_{load} < 100\ \mu\mathrm{m\,s}^{-1}$, as used experimentally, $V_{load}^2/D_0 \lesssim 10^{-3} g \ll \mu_s g$, which ensures that the inertial force $W\ddot{x}/g$ remains negligible when compared to the friction one $\mu_s W$. The dominant (longer) time scale is therefore t^* as stated.

[30] M. L. Falk and J. S. Langer, Phys. Rev. E **57**, 7192 (1998).

[31] K. L. Johnson, *Contact Mechanics* (Cambridge University Press, Cambridge, England, 1985).

[32] G. He, M. H. Müser, and M. O. Robbins, Science **284**, 1650 (1999).